Genetic resistance to yellow rust infection of the wheat ear is controlled by genes controlling foliar resistance and flowering time

Laura Bouvet[1,2], Simon Berry[3], Paul Fenwick[3], Sarah Holdgate[1], Ian J. Mackay[1†], James Cockram[1*]

[1]NIAB, 93 Lawrence Weaver Road, Cambridge, CB3 0LE, United Kingdom

[2]Department of Plant Sciences, University of Cambridge, Downing Street, Cambridge, CB2 3EA, United Kingdom

[3]Limagrain UK Ltd, Market Rasen, LN7 6DT, United Kingdom

[†]Current address: SRUC, The King's Buildings, West Mains Road, Edinburgh, EH9 3JG, United Kingdom

[*]Corresponding author: james.cockram@niab.com

Abbreviations

BLUEs	Best Linear Unbiased Estimators
MAGIC	Multi-parent advanced generation inter-cross
MAS	Marker-assisted selection
Pst	*Puccinia striiformis* f. sp. *tritici*
QTL	Quantitative trait locus
RIL	Recombinant inbred line
SNP	Single nucleotide polymorphism
YR	Yellow rust

Key words: Bread wheat (*Triticum aestivum* L.), yellow rust, stripe rust, glume infection, quantitative trait loci (QTL), multi-parent advanced generation inter-cross (MAGIC), marker-assisted selection (MAS), single nucleotide polymorphism (SNP)

Core ideas

- *Puccinia striiformis* f. sp. *tritici* (*Pst*) causes yellow rust (YR) in wheat leaves.
- We present the first reports for the genetic control of YR on the wheat ear.
- Ear YR infection is controlled by subsets of QTL controlling leaf resistance and flowering time.
- The findings are relevant to wheat breeding for *Pst*-prone environments.

Abstract

Yellow rust (YR), or stripe rust, is a fungal infection of wheat (*Triticum aestivum* L.) caused by the pathogen *Puccinia striiformis* f. sp. *tritici* (*Pst*). While much research has focused on YR infection of wheat leaves, we are not aware of reports investigating the genetic control of YR resistance in other wheat structures, such as the ears. Here we use an eight-founder population to undertake genetic analysis of glume YR infection in wheat ears. Five quantitative trait loci (QTL) were identified, each explaining between 3.4% and 6.8% of the phenotypic variation. Of these, three (*QYrg.niab-2D.1, QYrg.niab-4D.1* and *QYrg.niab-5A.1*) co-located with QTL for leaf YR resistance previously identified in the same population. Additional leaf YR resistance QTL previously identified in the population were not detected as controlling glume resistance, with the remaining two glume YR QTL linked to genetic loci controlling flowering time. The first, *QYrg.niab-2D. 1*, mapped to the major flowering time locus *Photoperiod-D1* (*Ppd-D1*), with the early-flowering allele from the founder Soissons conferring reduced glume YR resistance. The second, *QYrg.niab-4A.1*, was identified in one trial only, and was located close to a flowering time QTL. This indicates earlier flowering results in increased glume YR susceptibility, likely due to exposure of tissues during environmental conditions more favourable for *Pst* infection. Collectively, our results provide first insights into the genetic control of YR resistance in glumes, ontrolled by subsets of QTL for leaf YR resistance and flowering time. This work provides specific genetic targets for the control of YR resistance in both the leaves and the glumes, and may be especially relevant in *Pst*-prone agricultural environments where earlier flowering is favoured.

Introduction

The fungal pathogen *Puccinia striiformis* f. sp. *tritici* (*Pst*) causes yellow rust (YR), also known as stripe rust, in wheat (*Triticum aestivum* L.). The visible symptoms of YR infection, such as sporulation, are typically observed on wheat leaves. However, under the right conditions *Pst* urediniospores will also colonise leaf sheaths, as well as structures of the wheat ear including the outermost structures that surround each floret (the glumes) (Figure 1a-b). While the main concern for wheat growers is foliar infection, glume infection can become a significant problem during moderate to severe epidemics. *Pst* uredinospores infect floret tissues from heading date (Zadoks Growth Stage 55, GS55; Zadoks et al. 1974) until flowering (GS61), with symptoms appearing 10 to 20 days later (Wellings, 2003). Inside each floret, *Pst* germination and sporulation will occur on glumes, lemma and palea. At a first glance, infected wheat heads appear discoloured or bleached, and symptoms can be mistaken for that of other diseases such as Fusarium head blight. Upon closer inspection, pustules inside the spikes are more evident and opening the floret exposes urediniospores, thereby confirming *Pst* infection. These symptoms are short-lived compared to foliar infection, mainly because cycles or re-infection are more difficult when spores are encased within the florets, and because they occur towards the end of the plant lifecycle, including fertilization and grain filling. An additional symptom includes shrivelled grains, although this is largely dependent on the timing on infection. Generally, the earlier the infection at the onset of flowering, the higher the extent of shrivelled grain. In severe cases, glume infection can lead to grain quality downgrading, as exemplified by reports of a 77% reduction in grain weight relative to uninfected plants (Cromey, 1989a) as well as a 20% yield reduction in a resistant variety (Purdy & Allan, 1965). *Pst* glume infection is mostly observed in varieties which are moderately to highly susceptible to YR infection of the leaf (Wellings, 2003). Thus, a variety with foliar resistance will generally also show resistance in the ear, while a susceptible variety is much more likely to exhibit symptoms of glume infection. However, there have been reports of moderately resistant varieties exhibiting unusually high levels of glume infection (Cromey, 1989b; Purdy & Allan, 1965; Wellings, 2003, 2009). While little is known about the effects of environmental conditions, ear morphology and the timing of flowering on YR glume infection, reports suggest that moisture and cool temperatures at flowering are key factors in the onset of significant outbreaks, and that florets are least susceptible after anthesis (Cromey, 1989a).

Pst infection of the leaves prevents leaf tissue from photosynthesizing. Extensive infection of the ears may have a similar detrimental effect on photosynthesis, particularly when leaf photosynthetic area is already significantly reduced due to extensive sporulation, necrosis and/or chlorosis. Ear photosynthesis significantly contributes towards grain filling by providing the developing grain with an important source of photoassimilates (10-76 %) and has been shown to exhibit similar levels of CO_2 fixation to the flag leaf (Maydup et al. 2010; Tambussi et al. 2007). These characteristics are particularly relevant under drought conditions, when ears exhibit higher water use efficiency than flag leaves (Tambussi et al. 2007). The photosynthetic capacity of ears has therefore been recognised as an area relevant to wheat breeding and is the target of further optimisation as part of international research efforts looking to increase wheat yield potential, such as the Wheat Yield Consortium (Parry et al. 2011). In addition, if we consider the ways in which *Pst* uredinospores can colonise plant tissue, glume infection could potentially pose a threat to hybrid wheat breeding: as wheat is a predominantly inbreeding crop, developing hybrids requires male sterility in female parents, which receive pollen from male parents. This critical cross-pollination step relies on open florets during anthesis, providing an easy entry point for *Pst* urediniospores. In the context of a moderate to severe yellow rust outbreak, glume infection could result in increased levels of shrivelled grain, posing a serious problem for the large-scale seed multiplication efforts required by commercial hybrid breeding.

More than 300 genetic loci controlling resistance to foliar YR infection have been identified, of which around 80 represent permanently named yellow rust resistance (*Yr*) genes (summarised by Jamil et al. 2020). However, the genetic components underlying glume resistance have not been explored, with current knowledge essentially limited to its phenotypic symptoms. Here we use an eight-parent wheat multi-founder advanced generation inter-cross (MAGIC) population genotyped using a 90,000 feature single nucleotide polymorphism (SNP) array which has previously been used for genetic mapping of YR infection of the leaf (Bouvet et al. 2021) to: (1) characterise for the first time the genetic basis of glume YR resistance, and (2) compare glume resistance QTL to the genetic basis of yellow rust resistance in leaves.

Methods

Wheat germplasm and field trials

The eight-founder 'NIAB Elite MAGIC' wheat population is previously reported (Mackay et al. 2014). Briefly, it consists of eight founders (the varieties Alchemy, Brompton, Claire, Hereward, Rialto, Robigus, Soissons and Xi19) inter-crossed over three generations, after which >1,000 recombinant inbred lines (RILs) were developed by inbreeding. A subset of the population was sown in two untreated, partially replicated trials sown in the autumn of 2015, and grown to maturity to the following summer of 2016. The trial sites were in the United Kingdom (UK) at NIAB in Cambridgeshire (NIAB16; latitude 52.235010, longitude 0.097871) and Osgodby in Lincolnshire (OSG16; latitude 53.410161, longitude -0.386770). Each trial consisted of 1,200 plots arranged in 20 columns and 60 rows. Trial design consisted of 2 main-blocks, with 3 blocks and 2 sub-blocks per block, containing 444 MAGIC RILs in two replicates and 234 un-replicated RILs. Trial designs were generated using DEW experimental design software (www.expdesigns.co.uk). Each RIL was sown in two 1-m rows, with six rows sown adjacent to each other at a time, thus forming 1x1m areas consisting of three RILs and/or founders. At NIAB16, the central two rows were sown with the YR susceptible variety, Vuka, which served to help spread YR infection. In contrast, at OSG16, 1x1 m plots of Vuka were sown every three traverses. NIAB16 was artificially inoculated with a mixture of *Pst* races: 'Solstice' (isolate 08/21 virulent on *Yr 1, 2, 3, 4, 6, 9, 17, 25, 32*) and 'Warrior' (isolate 11/08 virulent on *Yr 1, 2, 3, 4, 6, 7, 9, 17, 25, 32, Sp*). For OSG16, no inoculation was undertaken. Both trials were subjected high levels of natural *Pst* inoculum early in the season, and it is therefore highly likely that both sites were predominantly exposed to the effects of natural *Pst* infection. Based on UK Cereal Pathogen Virulence Survey (UKCPVS) data of *Pst* isolates in 2016, Cambridgeshire and Lincolnshire (including samples from the Osgodby site) were dominated by the Warrior group of races (UKCPVS, 2017) (Supplementary Table 1).

Glume YR assessment and phenotypic data analysis

Glume infection was assessed at the late milk development stage (GS77). For each plot, 10-12 ears were selected at random and the number of spikelets per ear exhibiting glume infection counted. This was converted into a percentage to obtain an estimate of the proportion of ear infection, which was assigned a number on a five-point scale from 0-4, where 0 represents no infection and 4 represents all glumes per head infected (Table 1). A score was allocated when ≥50 % of the ears within a plot corresponded to that score. Linear mixed models based on

Restricted Maximum Likelihood (REML) were used to adjust the infection data and take in account any spatial variation. Best Linear Unbiased Estimators (BLUEs) were computed following a step-wise model selection approach. Baseline models considered were as follows: Model 1 – Blocking: genetic effects are estimated based only on the inter- and intra-block variation recovered from the model. Model 2 – spatial: only considers global and/or local field trends. Model 3 - spatial + blocking: combination of the above models. Models were fitted using Genstat 18th edition (VSN International, 2015). Akaike Information Coefficient (AIC) was used as a measure for model selection (Akaike, 1974): each model was optimised using AIC as a measure of model fit, and the model with the lowest AIC value selected. Inspection of the glume infection distribution and residual plots revealed a dataset skewed towards resistance. Therefore, the natural log was applied to improve the normality of the data. Phenotypic data for YR infection of the leaf in the NIAB16 and OSG16 trials has previously been reported, as part of a wider series of five trials investigating the genetics of foliar YR infection (Bouvet et al. 2021). To determine the consistency of the phenotype across test environments, and the relationship between YR glume infection with YR leaf infection previously reported in the same trials (Bouvet et al. 2021), Pearson correlation coefficients for glume infection were computed using the 'cor.test()' function in the statistical software R 3.6.1 (R Core Team, 2019).

Genetic analyses and bioinformatics

The MAGIC population was previously genotyped using a 90,000 feature Illumina SNP array (Wang et al. 2014), as described by Mackay et al. (2014), and a MAGIC genetic map subsequently generated (Gardner et al. 2016). QTL analysis was undertaken following four different statistical methods. Method 1 - single marker analysis (SMA): regression analysis on allelic state of 7,369 mapped SNP markers from the MAGIC genetic map. The remaining analyses were based on founder haplotype probabilities calculated with the 'mpprob' function in R/mpMap (Huang et al. 2011) with a threshold of 0.5. Method 2 – identity by descent (IBD): regression analysis on founder haplotype probabilities using R/qtl. Method 3 - interval mapping (IM): conducted in R/mpMap using the haplotype probability estimates. Method 4 - composite interval mapping (CIM): as IM but with 10 marker covariates. Empirical p=0.05 significance thresholds for IM were computed in R/mpMap using the 'sim.sig.thr' function, producing a cut-off at p=1.6E-05 (-log10(p)=4.8) for NIAB16 and p=3.7E-05 (-log10(p)=4.2) for OSG16. For IM and CIM, QTL were fitted with p<0.05 and with phenotypic variance explained (PVE)>0.5%. For SMA and IBD, the package R/qvalue was used to correct for multiple testing,

with a *q*-value threshold of 0.05 (R Core Team, 2017). QTL intervals were defined as a genomic region which, at a given genetic position had a *q*-value ≤1.6E-05 (NIAB16) and *q*≤ 3.7E-05 (OSG16). The genetic versus physical map location of each QTL was determined for each relevant chromosome by plotting the location of SNPs on the MAGIC genetic map (Gardner et al. 2016) against their position on the physical map of the wheat reference genome assembly (RefSeq v1.0; IWGSC et al. 2018) and the location of the most significant SNP for a given QTL highlighted. Data were plotted using R/ggplot2 (Wickham, 2009).

Results

MAGIC population response to Pst glume infection

Genotyped MAGIC lines were assessed for YR disease severity in the ears (Figure 1a-b) at two test environments in 2016: trials NIAB16 and OSG16. Amongst the MAGIC founders, cv. Soissons showed high glume YR infection in both trials (mean >2.5; Figure 1c). The remaining seven founders were found to be relatively resistant, with mean glume infection (GIF) scores ≤1, with Xi19 showing the second highest founder glume infection in both trials. The MAGIC RILs showed phenotypic variation over the full range of the assessment scale (Figure 1c): nearly 70 % of RILs showed little or no infection (GIF = 0) while ~10 % exhibited *Pst* infection in the majority of the ear (GIF = 3-4) (Supplementary Figure 1). Pearson's correlation coefficient analysis of the MAGIC glume YR infection data alongside previously reported leaf YR infection data from the same trials (Bouvet et al. 2021) found a positive correlation at both environments, with OSG16 (R=0.62, p<2.2E-16) showing a stronger correlation than was observed at NIAB16 (R=0.49, p<2.2E-16) (Figure 2). MAGIC RILs susceptible in the glumes generally also exhibited high leaf susceptibility (leaf infection >60%). However, a few notable exceptions were observed, particularly at NIAB16 where six RILs (accessions 5954, 6216, 5770, 5883, 6110, 6374) were found to be moderately resistant on leaves (infection score ≤25%) but susceptible in the glumes (GIF >3.5). One these, RIL 5954 displayed the same phenotypic combination at OSG16. Glume YR phenotypic data is listed in Supplementary Table 2.

Statistical analysis of the glume infection phenotypic data using REML showed that the Wald statistic for genotype effect was highly significant (Chi pr <0.001) at both environments (Supplementary Table 3). High genotypic performance is further supported by high broad sense heritability values at NIAB16 (h^2=0.80) and OSG16 (h^2=0.82), mirroring values observed for leaf infection at the same trials (h^2=0.79-0.94) (Bouvet et al. 2021). This evidence points towards stable genotypic performance for glume infection in the MAGIC population at each site. However, the weaker correlation of glume infection scores between OSG16 and NIAB16 (R=0.47, p<2.2E-16) highlights possible genetic x environmental interaction (Supplementary Figure 2).

MAGIC QTL mapping of glume YR resistance and comparison with leaf YR resistance QTL

Five glume YR resistance QTLs were identified, located on chromosomes 2D (*QYrg.niab-2D.1*), 4A (*QYrg.niab-4A.1*), 4D (*QYrg.niab-4D.1*) and 5A (*QYrg.niab-5A.1*), as listed in Table 2, with MAGIC founder effects at each QTL summarised in Table 3. Marker-by-marker results of all genetic mapping methods are listed in Supplementary Table 4. The percentage of the phenotypic variance explained (PVE) for each QTL was around 5%, ranging from 3.4 to 6.8%, and jointly accounting for ~23% PVE. For each QTL, placing the peak SNP on plots of genetic versus physical map positions for all other markers on the corresponding chromosomes allowed QTL locations to be viewed in genomic context (Figure 3). Four of the five QTL were located on the long arms of their respective chromosomes in regions of high genetic recombination, ≤43 Mbp from the telomere. Indeed, *QYrg.niab-4D.1* (4.8% PVE), *QYrg.niab-2D.1* (3.9% PVE) and *QYrg.niab-5A.1* (6.8% PVE) were located very close to the ends of their chromosomes, just 7, 13 and 19 Mbp from the chromosome 4D, 2D and 5A telomeres, respectively. *QYrg.niab-4A.1* (3.4 % PVE) was ~39 Mbp from the chromosome 4A long arm telomere and was located within a region of low agreement between SNP genetic versus physical map order. A region on chromosome 4A from 170-210 cM has previously been identified as a region of unusually high marker density and high segregation distortion against alleles from the founder Robigus (Gardner et al. 2016). Robigus is thought to have the related wheat species *Triticum dicoccoides* in its pedigree, and the 170-210 cM region in the MAGIC map has been previously identified as one of two chromosomal segments from *T. dicoccoides* segregating in the population via Robigus (Gardner et al. 2016). However, the glume YR resistance allele at *QYrg.niab-4A.1* is predicted to be conferred by Xi19, and so does not originate from the alien introgression. *QYrg.niab-2D.PpdD1* (6.4% PVE) was located half way down the chromosome 2D short arm in a region of high genetic recombination.

Our previous study reported leaf YR resistance QTL at five sites using the MAGIC population, which included the NIAB16 and OSG16 trials investigated here for glume YR resistance (Bouvet et al. 2021). Cross-comparison between the glume and YR resistance QTL showed three of our glume QTL to co-locate with leaf QTL: (1) glume QTL *QYrg.niab-2D.1* and leaf QTL *QYr.niab-2D.1* (~18% PVE; Bouvet et al. 2021), both identified by the same peak marker (*Ra_c21099_1781*). (2) Glume QTL *QYrg.niab-4D.1* and leaf QTL *QYr.niab-4D.1* (4% PVE; Bouvet et al. 2021), both defined by the same peak marker (*D_GDRF1KQ02H66WD_341*). (3) Glume QTL *QYrg.niab-5A.1* and leaf QTL *QYr.niab-5A.1* (3.6% PVE; Bouvet et al. 2021), for which the peak markers were 8 cM apart. For the remaining two glume resistance QTL, the peak marker for *QYrg.niab-2D.Ppd_D1* was a diagnostic causative marker within the

Photoperiod-D1 (*Ppd-D1*) gene, which distinguishes the early flowering photoperiod insensitive Soissons *Ppd-D1a* allele from the photoperiod sensitive *Ppd-D1b* alleles at the remaining seven founders (Bentley et al. 2013). Allelic effects at *QYrg.niab-2D.Ppd_D1* showed increased glume YR susceptibility was conferred by the Soissons allele. Finally, *QYrg.niab-4A.1*, identified in NIAB16 only and explaining 3.4 % PVE, was not found to co-locate with any QTLs for yellow rust resistance in leaves. Glume QTL *QYrg.niab-4A.1* did not co-locate with any of the MAGIC leaf YR resistance QTL identified by Bouvet et al. (2021).

Discussion

Wheat ear photosynthetic capacity plays a significant role in grain filling (Wang et al. 2016), particularly under stress conditions (Tambussi et al. 2007). While ear YR infection may not currently be as much of a recurrent problem as leaf infection, at least in the European context, it can become detrimental to yields provided suitable growing and environmental conditions. Due to climate change, temperatures are predicted to rise in many of the wheat growing areas of the world (IPCC, 2019). Such changes, including during the important wheat developmental stages of ear emergence, flowering and early grain fill, may result in wheat pests and diseases posing a greater, or changing, threat to optimum wheat grain yields. Indeed, simulations of UK wheat development under greenhouse gas emission scenarios finds acceleration of days to anthesis to accelerate by 13-19 days (Harkness et al. 2020). Despite such current and future risks, no previous reports of the genetic basis of wheat ear YR resistance have been published. Here, we begin to address this knowledge gap, finding that glume YR infection is controlled by a subset of genetic loci that confer resistance to foliar YR infection, combined with pleiotrophic effects of loci controlling the timing of ear emergence and subsequent development. Below we explore in more detail some of the issues related to these findings.

Glume YR infection and phenotype

Variation for ear infection in the MAGIC population was skewed towards resistance, with the majority of MAGIC RILs showing little-to-no yellow rust infection. This trend is different to that observed for foliar infection reported in the same trials, which exhibited a less skewed range of phenotypic variation (Bouvet et al. 2021). Assessing the extent of yellow rust infection in ears is harder compared to foliar infection, as disease symptoms are more easily and rapidly identified on leaves. Here, the degree of difficulty in phenotypic assessment had to be balanced with the practicalities of scoring large numbers of plots in the field. Therefore, a simple 0-4 scale was developed, which would have inevitably grouped together finer levels of response. Notably, infection may have been missed completely if it was confined to the inner layers of the floret which are not visible without manual intervention. This may partly explain the relatively low correlation between leaf and glume infection (NIAB16 R=0.49; OSG16 R=0.62), and on the power and precision to identify QTL. Leaf and ear infection not only differed in phenotypic distribution, but also in broad sense heritability: ear infection exhibiting >10% lower heritability in both environments, indicating additional non-genetic factors have a larger impact on the phenotypic response in ears than in leaves, and/or that the limitations of

the 0-4 glume infection scale combined with the inherent difficulty in accurately scoring glume infection impacted phenotyping accuracy. This difference in heritability is in agreement with YR resistance studies in Triticale (a hybrid between wheat and rye) that also report lower heritability in ears compared to leaves (Losert et al. 2017). Furthermore, Losert et al. (2017) argue that the severe ear infection they observed in Triticale may have been a feature of the prevalent *Pst* 'Warrior' race and its potential ability to develop at warmer temperatures. Although temperature adaptation of the 'Warrior' race variants have not been experimentally confirmed, as they have for the aggressive race *Pst*S2 for example (Milus et al. 2009), it is plausible that warmer temperatures not previously conducive of germination and subsequent colonisation enable the pathogen to prolong its growth into photosynthetic tissue later in the season, such as the glumes (Mboup et al. 2012). The UK regions in which the trials were conducted were dominated by the 'Warrior' group of *Pst* races (Hubbard et al. 2017; Supplementary Table 1). Indeed, 2016 was a year that saw a high number of yellow rust infected leaf samples received by the UK Cereal Pathogen Virulence Survey, with some samples received as early as January (Hubbard et al. 2017). In addition to inoculum levels, other factors may explain between site differences in glume YR infection. For example, climatic differences may have played a role, with the OSG16 trial located in a cooler and wetter region than the NIAB16 trial. This likely led to a longer window of infection for *Pst* urediniospores, making disease symptoms more pronounced and easier to score later in the season, thus resulting in a stronger correlation between leaf and ear infection. Overall, our observations were in line with reports that ear YR infection is prominent when significant levels of inoculum are present and are coupled with suitable growing conditions and timely flowering (Cromey, 1989a; Wellings, 2003).

The role of foliar YR resistance loci in glume resistance

The co-location of three of our five glume YR QTL with foliar resistance QTL previously identified in the same trials (Bouvet et al. 2021) indicates the presence genetic mechanisms in common. Based on the percentage of the phenotypic variance explained, the leaf YR QTL identified in the MAGIC population by Bouvet et al. (2021) were classified as either 'major' (>5% PVE, 8 QTL) or 'minor' (<5% PVE, 6 minor QTL). Interestingly, only one of the three glume YR QTL corresponded to a 'major' foliar YR locus: *QYrg.niab2D.1* (glume 3.9% PVE) versus *QYr.niab-2D.1* (leaf 18% PVE). The finding that the remaining two glume resistance loci corresponded to minor foliar leaf QTL, and that none of the remaining seven 'major' foliar resistance loci (each controlling 6-17% foliar PVE) were relevant in the glumes, was somewhat

unexpected. Together this indicates that while genetic mechanisms are shared between glume and leaf YR resistance, the importance of specific genetic loci in controlling these resistances is different between the two tissues. This finding has implications for breeding targets for current agricultural environments conductive to late *Pst* pressure, for environments likely to become higher risk due to changes in climate, or for the use of earlier flowering varieties.

A role for phenology in glume YR resistance

Ear infection by *Pst* commonly affects susceptible wheat varieties. However, YR ear infection of relatively resistant wheat varieties has been reported in New Zealand (Cromey, 1989b). This phenomenon was observed in the MAGIC founder Soissons, which was very susceptible to *Pst* glume infection (Figure 1c) but had very high leaf resistance (Bouvet et al. 2021). While this difference could be due to several factors, Soissons is notable amongst the MAGIC founders for its early flowering phenotype - due largely to carrying the photoperiod insensitive early-flowering *Ppd-D1a* allele. The most significant SNP for the glume YR QTL *QYrg.niab-2A.PpdD1* was within the *Ppd-D1* gene, and represents a diagnostic marker that discriminates between the early flowering Soissons allele and the late-flowering allele(s) carried by the remaining seven MAGIC founders. As the early *Ppd-D1a* allele was associated with increased glume YR susceptibility, early flowering likely effects glume susceptibility pleiotropically. Further evidence of a link between YR ear infection and flowering time was provided by the co-location of *QYrg.niab-4A.1* with the multi-year, multi-location flowering time QTL *QFt.niab-4A.03*, previously identified in the same MAGIC population (Ian Mackay, personal communication). An influence of flowering time on glume YR infection was somewhat expected, as flowering time often influences other fungal diseases of the wheat ear. While earlier flowering was associated with increased glume YR infection, early varieties often come with other benefits. These include avoidance of fungal diseases of the ear such as fusarium head blight (Gervais et al. 2003) and Septoria nodorum glume blotch (Aguilar et al. 2005; Downie et al. 2020; Lin et al. 2020a, 2020b; Scott et al. 1982), as well as drought avoidance. Early flowering can also be beneficial due to agronomic considerations, such as the timing and logistics of harvest. Therefore, despite evidence UK wheat varieties released over the last 10 years have an increasingly narrower range of phenology with a much smaller proportion of early varieties currently available (Sheenan & Bentley, 2020), there is still demand for early varieties - which accounted for 14% of certified UK seed weight in 2019 (NIAB TAG, 2020).

Conclusions

This study provides a starting point towards understanding the genetic components underlying YR resistance in wheat glumes, how it relates to foliar resistance, and demonstrates that subsets of genetic loci controlling flowering time likely also have a pleiotropic effect. The knowledge of which QTLs are relevant to both leaf and glume resistance will help inform marker-assisted breeding approaches best suited for wheat varieties for growth in agricultural environments in which glume *Pst* infection is prevalent.

Acknowledgements

LB was funded via a Biotechnology and Biological Sciences Research Council (BBSRC) Doctoral Training Partnership PhD award to the University of Cambridge. LB also received funding from the Roger Harrison Trust towards travel expenses. We thank Prof Julian Hibberd (University of Cambridge) for supervisory inputs within the Doctoral Training Programme and the NIAB Trials Team for the sowing, growth and agronomic care of the NIAB field trail.

Author contributions

LB carried out trial preparation, pathology work, yellow rust assessments and all statistical and genetic analyses. SB and PW managed the trial at Osgodby. IM, SH and JC provided project supervision and resources. LB wrote the manuscript, with input from JC. All authors edited and approved the manuscript.

References

Aguilar V, Stamp P, Winzeler M, Winzeler H, Schachermayr G, Keller B, Zanetti S, Messmer MM (2005) Inheritance of field resistance to Stagonospora nodorum leaf and glume blotch and correlations with other morphological traits in hexaploid wheat (*Triticum aestivum* L.). Theor Appl Genet 11:325–336

Bentley AR, Jensen EF, Mackay IJ, Hönicka H, Fladung M, et al. (2013) Flowering time. In: Cole C (ed) Genomics and breeding for climate resilient crops: target traits, vol 2. Springer-Verlag, pp 1-66

Bostwick DE, Ohm HW, Shaner G (1993) Inheritance of Septoria glume blotch resistance in wheat. Crop Sci 33:439–443

Bouvet L, Percival-Alwyn L, Berry S, Fenwick P, Mantello CC, Holdgate IJ, Cockram J (2021) Wheat genetic loci conferring resistance to yellow rust in the face of recent epidemics of genetically diverse races of the fungus *Puccinia striiformis* f. sp. *tritici*. Research Square, doi: 10.21203/rs.3.rs-459064/v1.

Cockram J, Mackay I (2018) Genetic mapping populations for conducting high-resolution trait mapping in plants. In: Varshney R, Pandey M, Chitikineni A (eds) Plant genetics and molecular biology. Advances in Biochemical Engineering/Biotechnology, vol 164. Springer, Cham.

Cromey MG (1989a) Occurrence and effects of stripe rust in wheat spikes in New Zealand. New Zeal J Crop Hort Sci 17:155–158

Cromey MG (1989b) Infection and control of stripe rust in wheat spikes. New Zeal J Crop Hort Sci 17:159-164

Downie RC, Lin M, Borsi B, Ficke A, Lillemo M, Oliver RP, Phan H, Tan K-C, Cockram J (2020) Spetoria nodorum blotch of wheat: disease management and resistance breeding in the face of shifting disease dynamics and a changing environment. Phytopathol doi: https://doi.org/10.1094/PHYTO-07-20-0280-RVW

Gardner KA, Wittern LM, Mackay IJ (2016) A highly recombined, high-density, eight founder wheat MAGIC map reveals extensive segregation distortion and genomic locations of introgression segments. Plant Biotechnol J 14:1406-1417

Gervais L, Dedryver F, Morlais J-Y, Bodusseau V, Negre S, Bilous M, Groos C, Trottet M (2003) Mapping of quantitative trait loci for field resistance to Fusarium head blight in an European winter wheat. Theor Appl Genet 106:961–970

Harkness C, Semenov MA, Areal F, Senapati N, Trnka M, Balek J, Bishop J (2020) Adverse weather conditions for UK wheat production under climate change. Agric For Meteorol 282-283:107862

Hubbard A, Wilderspin S, Holdgate S (2017) United Kingdom Cereal Pathogen Virulence survey 2017 Annual Report. NIAB

The International Wheat Genome Sequencing Consortium (IWGSC), Appels R, Eversole K, Stein N, Feuillet C, Keller B, Rogers J Pozniak C, et al. (2018) Shifting the limits in wheat research and breeding using a fully annotated reference genome. Science 361:eaar7191

Jamil S, Shahzad R, Ahmad S, Fatima R, Zahid R, Anwar M, Iqbal MZ, Wang X (2020) Role of genetics, genomics and breeding approaches to combat stripe rust of wheat. Front Nutr 7:580715

Lin M, Corsi B, Ficke A, Tan K-C, Cockram J, Lillemo M (2020a) Genetic mapping using a wheat multi-founder population reveals a locus on chromosome 2A controlling resistance to both leaf and glume blotch caused by the necrotrophic fungal pathogen *Parastagonospora nodorum*. Theor Appl Genet 133:785-808

Lin M, Stadlmeier M, Mohler V, Tan K-C, Ficke A, Cockram J, Lillemo M (2020b) Identification and cross-validation of genetic loci conferring resistance to Septoria nodorum blotch using a German multi-funder winter wheat population. Theor Appl Genet 134:125-142

Losert D, Maurer HP, Leiser WL, Würschum T (2017) Defeating the Warrior: genetic architecture of triticale resistance against a novel aggressive yellow rust race. Theor Appl Genet 130:685–696

Mackay IJ, Bansept-Basler P, Barber T, Bentley AR, Cockram J, Gosman N, Greenland AJ, Horsnell R, Howells R, O'Sullivan DM, Rose GM, Howell PH (2014) An eight-parent multiparent advanced generation inter-cross population for winter sown wheat: creation, properties, and validation. G3: Genes Genomes Genet 4:1603–1610

Maydup M, Antonietta M, Guiamet J, Graciano C, López JR, Tambussi EA (2010) The contribution of ear photosynthesis to grain filling in bread wheat (*Triticum aestivum* L.). Field Crops Res 119:48–58

Mboup M, Bahri B, Leconte M, de Vallavieille-Pope C, Kaltz O, Enjalbert J (2012) Genetic structure and local adaptation of European wheat yellow rust populations: the role of temperature-specific adaptation. Evol Appl 5:341–352

Milus EA, Kristensen K, Hovmøller MS (2009) Evidence for increased aggressiveness in a recent widespread strain of *Puccinia striiformis* f. sp. *tritici* causing stripe rust of wheat. Phytopathol 99:89–94

Nelson LR, Gates CE (1982) Genetics of host plant resistance of wheat to Septoria nodorum. Crop Sci 22:771–773

NIAB-TAG (2020) Seed production booklet. Certification statistics for England and Wales. Issue 103. January 2020. Available as part of NIAB-TAG Seeds Membership Package from niabtagnetwork@niab.com

Parry MAJ, Reynolds M, Salvucci ME, Raines C, Andralojc PJ, Zhu X-G, Price GD, Condon AG, Furbank RT (2011) Raising yield potential of wheat. II. Increasing photosynthetic capacity and efficiency. J Exp Bot 62:453–467

Purdy LH, Allan RE (1965) Stripe rust head infection in five Pacific northwest wheats. Plant Disease Reporter 49:335–338

R Core Team (2013) R: A language and environment for statistical computing. R Foundation for Statistical Computing, Vienna, Austria. URL http://www.R-project.org/

Scott PR, Benedikz PW, Cox CJ (1982) A genetic study of the relationship between height, time of ear emergence and resistance to Septoria nodorum in wheat. Plant Pathol 31:45-60

Scott M, Ladejobi O, Sammer A, Bentely AR, Biernaskie J, Bowden SA, Dell'Acqua M, Dixon LE, Filippi CV, Fradgley N, Gardner KA, Mackay IJ, O'Sullivan D, Percival-Alwyn L, Roorkiwal M, Singh RK, Thudi M, Varshney RK, Venturini L, Whan A, Cockram J, Mott R (2020) Multi-parent populations in crops: a toolbox integrating genomics and genetic mapping with breeding. Heredity 125:396-416

Shankar M, Walker E, Golzar H, Loughman R, Wilson RE, Francki MG (2008) Quantitative trait loci for seedling and adult plant resistance to Stagonospora nodorum in wheat. Phytopathol 98:886–893

Sheenan H, Bentley A (2020) Changing times: opportunities for altering winter wheat phenology. Plants People Planet 3:113-123.

IPCC (2019) Climate change and land: an IPCC special report on climate change, desertification, land degradation, sustainable land management, food security, and greenhouse gas fluxes in terrestrial ecosystems. Shukla PR, Skea J, Calvo Buendia E, Masson-Delmotte V, Pörtner H-O, et al. (eds). In press.

Tambussi EA, Bort J, Guiamet JJ, Nogués S, Araus JL (2007) The photosynthetic role of ears in C3 cereals: metabolism, water use efficiency and contribution to grain yield. Crit Rev Plant Sci 26:1–16.

Wang Y-Q, Xi W-X, Wang Z-M, Wang B, Xu X-X, Han M-K, Zhou S-L, Zhang Y-H (2016) Contribution of ear photosynthesis to grain yield under rainfed irrigation conditions for winter wheat cultivars released in the past 30 years in North China Plain. J Integr Agric 15:2247-2256.

Wellings CR (2003) Stripe rust head infection. Cereal Rust Report, 1:1–2.

Wellings CR (2009) Late season stripe rust damage: head infection and unpredicted variety responses. Cereal Rust Report 7:1–4

Zadoks Z, Chang TT, Konzak CF (1974) A decimal code for the growth stages of cereals. Weed Res 14:415-421

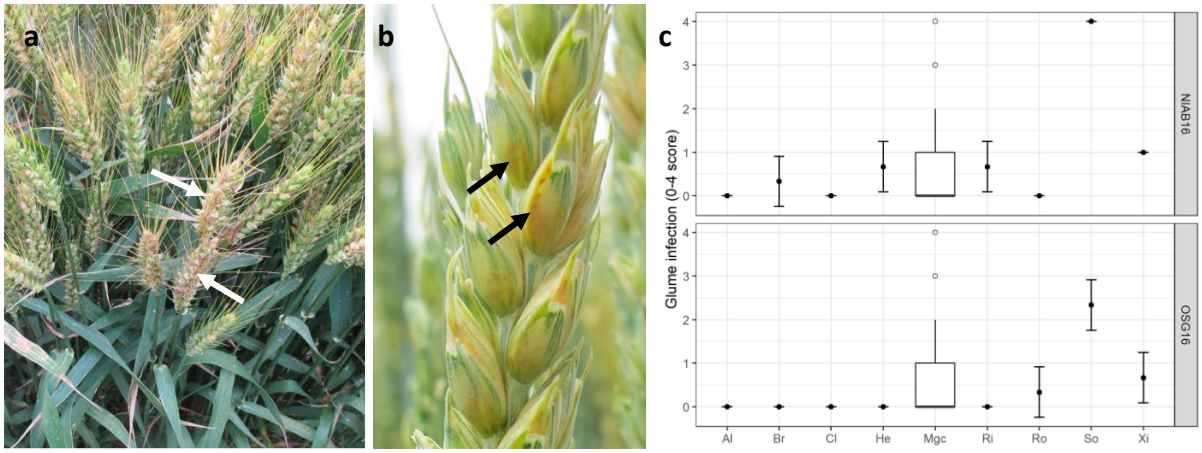

Figure 1. MAGIC founder yellow rust (YR) infection of the ear. Examples of founder Soissons at (A) the plot level, and (B) a close-up of a single ear. Arrows indicate example areas of notable infection, highlighting notable infections of the ear in general (white arrows) and the glumes (black arrows). (C) Distribution of glume YR infection of the MAGIC founders, and the MAGIC recombinant inbred lines (RILs) at the trials NIAB16 and OSG16. Mean glume infection is represented by filled black dots for each fonder, with standard deviation plotted as error bars. The central boxplot represents the distribution of the MAGIC RILs (single counts for un-replicated lines and total counts for replicated lines). Black unfilled circles represent outliers. MAGIC founders are listed as, Al: Alchemy, Br: Brompton, Cl: Claire, He: Hereward, Mgc: MAGIC RILs, Ri: Rialto, Ro: Robigus, So: Soissons, Xi: Xi19.

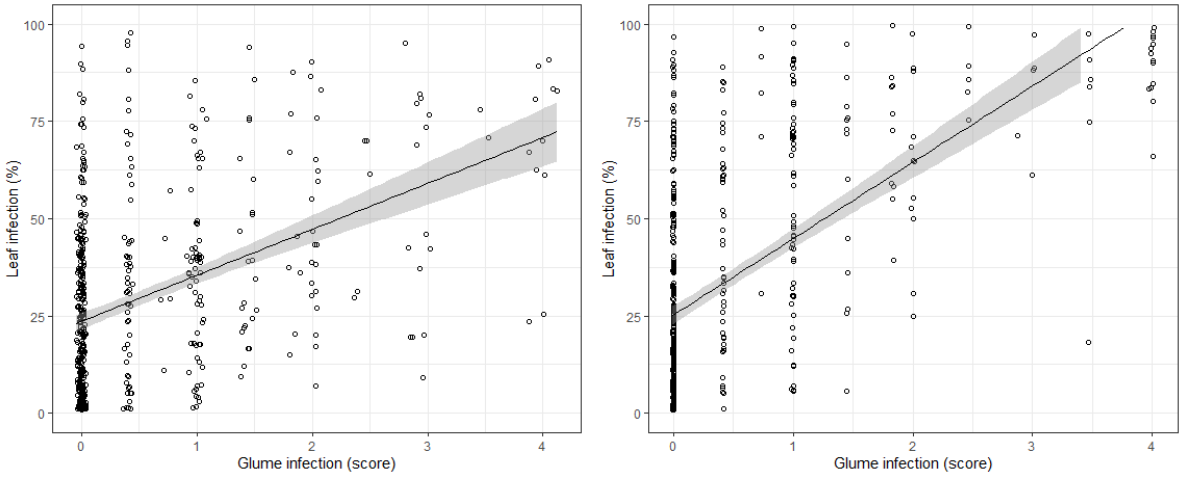

Figure 2. Correlation between MAGIC recombinant inbred line (RIL) yellow rust infection of the glume and the leaf at trials NIAB16 (left) and OSG16 (right). Back-transformed adjusted means were used for both scatter plots. The black line is the linear regression line and the grey area the 95 % confidence level interval. Pearson correlation coefficients: NIAB16: R=0.49, p<2.2E-16; OSG16: R=0.62, p<2.2E-16. Yellow rust leaf phenotypic data was sourced from Bouvet et al. (2021).

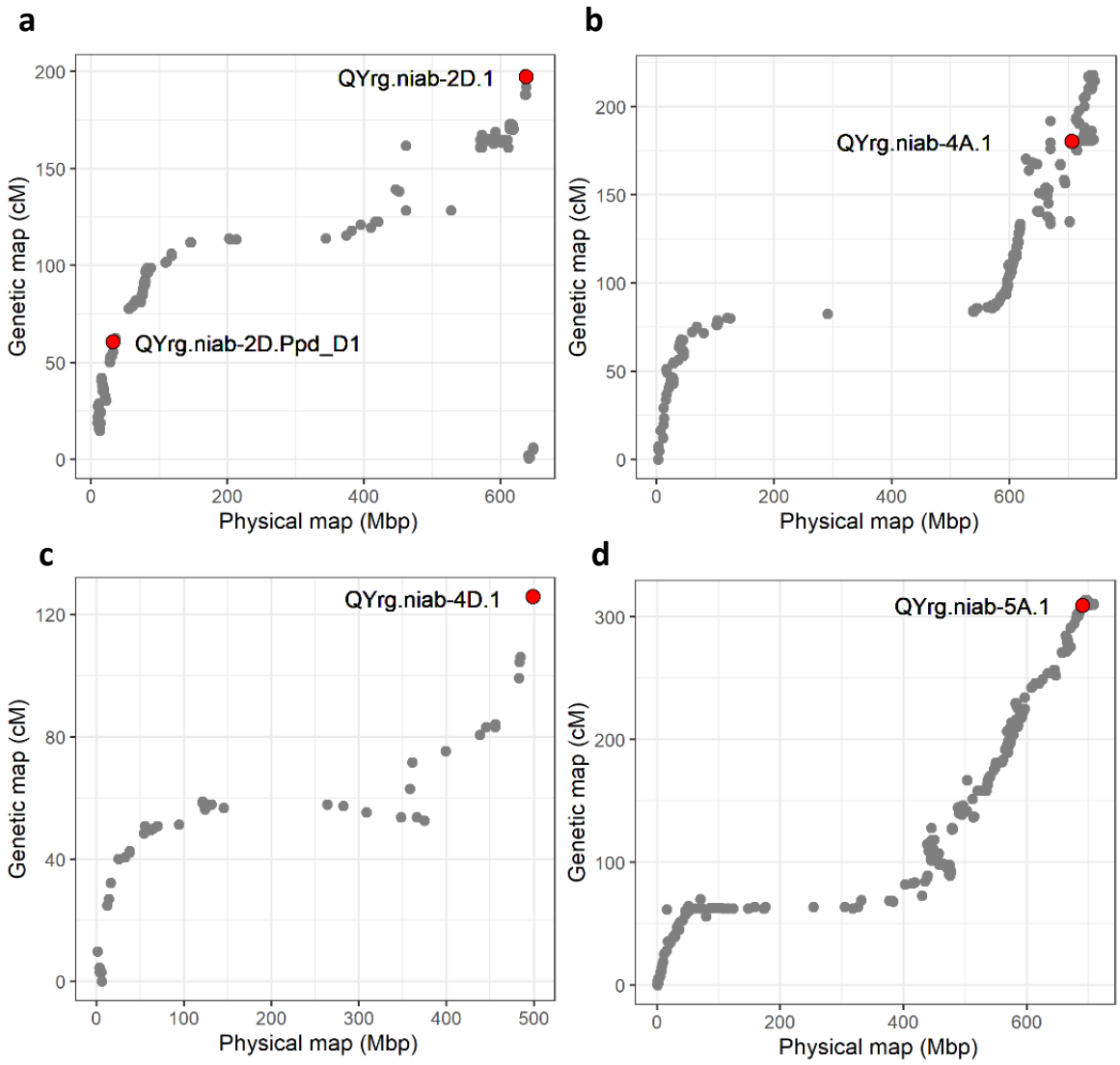

Figure 3. Genomic locations of the five quantitative trait loci (QTL) conferring glume yellow rust resistance in the MAGIC population. For each chromosome, plotted are the physical (Mbp; IWGSC, 2018) versus genetic (cM; Gardner et al. 2016) map positions of the genetic markers, with the peak marker locations for each QTL shown in red.

Score	YR ear infection
0	0%
1	25%
2	50%
3	75%
4	100%

Table 1. Scoring system used to phenotype yellow rust (YR) infection of the ear.

QTL	Chr.	Mapping method		Peak marker	Phys. pos. Mbp	Genetic pos. cM	*P*-value (trial, QTL mapping method used)		% PVE		QTL interval (cM)
		N16	**O16**				**min**	**max**	**min**	**max**	
QYrg.niab-2D	2D	3,4	4	*Ppd-D1*	34.0	60.67	4.61-07† (N16,3)	6.44E-05† (N16,4)	.	4.2†	11.88
QYrg.niab-2D.1	2D	4	3,4	*Ra_c21099_1781*	638.4	197.36	6.70E-06† (O16,4)	3.40E-04† (N16,4)	.	3.9†	10.85
QYrg.niab-4A.1	4A	3,4	.	*BS00067903_51*	705.6	180.38	.	3.80E-04† (N16,3)	.	3.5†	5.53
QYrg.niab-4D.1	4D	1-4	2-4	*D_GDRF1KQ02*‡	499.1	125.78	6.32E-08† (N16,4)	1.32E-05 (O16,4)	.	4.8†	.
QYrg.niab-5A.1	5A	1-4	2-4	BS00065714_51	691.0	309.03	9.12E-09 (N16,4)	3.98E-09† (O16,4)	6.2	6.8†	16.97

Table 2. Glume yellow rust (YR) resistance quantitative trait loci (QTL) identified in trials NIAB16 (N16) and OSG16 (O16). Glume QTL co-locating with previously identified leaf QTL (Bouvet et al. 2021) are underlined. QTL mapping methods are numbered as: (1) single marker analysis, (2) identity by descent, (3), interval mapping, and (4) composite interval mapping with 10 covariates. Minimum (min.) and maximum (max.) *p*-values for each QTL are indicated. Physical and genetic map information is from IWGSC (2018) and Gardner et al. (2016), respectively. †For each QTL, values for the percentage of the phenotypic variance explained (% PVE) correspond to the indicated *p*-value. QTL detected by method-4 only across both environments were not included. ‡Full marker name: *D_GDRF1KQ02H66WD_341*.

QTL	Chr.	Predicted founder effects								Trial, QTL method
		Al	Br	Cl	He	Ri	Ro	So	Xi	
QYrg.niab-2D	2D	0.09	0.01	-0.05	-0.04	0	0	0.3	0	NIAB16, 3
QYrg.niab-2D.1	2D	-0.24	0.09	-0.05	0.43	-0.32	-0.26	0.32	0	NIAB16, 4
QYrg.niab-4A.1	4A	-0.27	-0.18	-0.2	-0.34	-0.33	-0.32	-0.41	0	NIAB16, 3
QYrg.niab-4D.1	4D	0.23	-0.08	NA	0.32	0.55	0.52	0.4	0	OSG16, 3
QYrg.niab-5A.1	5A	-0.18	-0.12	-0.15	-0.31	0.07	-0.1	0.13	0	OSG16,4

Table 3. Predicted founder effects at the five quantitative trait loci (QTL) conferring glume yellow rust resistance, based on natural-log adjusted BLUEs. For each QTL, founder effects presented are for the consensus marker listed in Table 2 with the most significant *p*-value identified with QTL mapping method-3 (interval mapping) and method-4 (composite interval mapping with 10 covariates). MAGIC founders, Al: Alchemy, Br: Brompton; Cl: Claire, He: Hereward, Ri: Rialto, Ro: Robigus, So: Soissons, Xi: Xi19. Founder effects are all relative to those of Xi19.

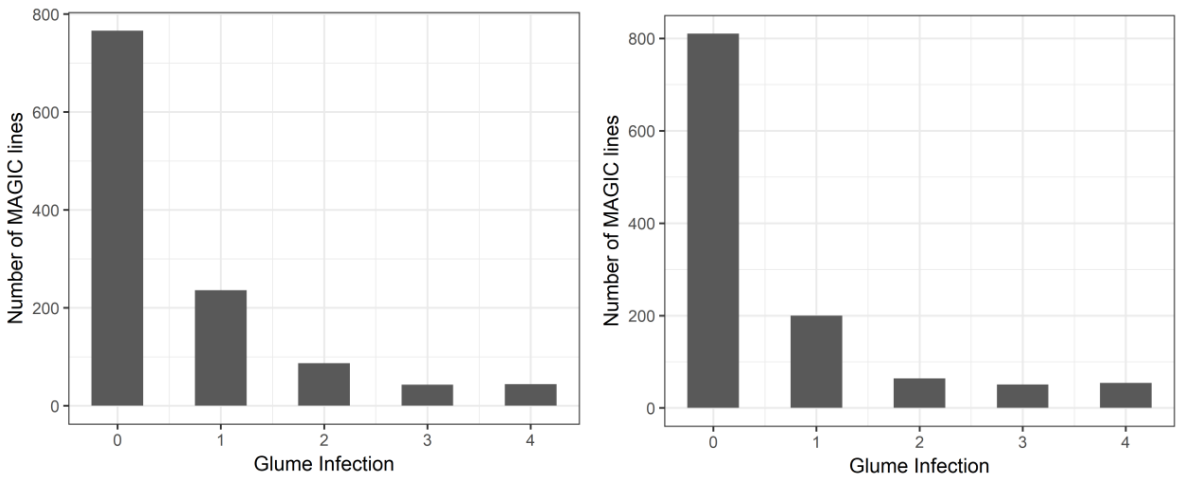

Supplementary Figure 1. Histogram of yellow rust glume infection in the MAGIC recombinant inbred lines (RILs) at trials NIAB16 (left) and OSG16 (right). The number of MAGIC RILs includes single counts for un-replicated lines and total counts for replicated lines.

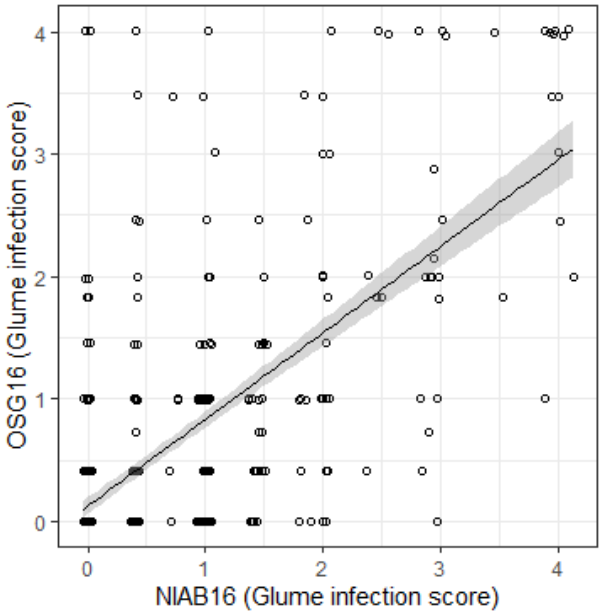

Supplementary Figure 2. Scatter plot showing the correlation between glume yellow rust infection at trial sites NIAB16 and OSG16. Scatter plot shows back-transformed adjusted means. The black line is the linear regression line and the grey area the 95% confidence level interval. Correlation coefficients: R=0.47, p<2.2E-16.

Location	Isolate code	Year	Pathotype
Cambridgeshire	16/009	2016	Red race 5 (Warrior group)
Cambridgeshire	16/048	2016	Pink (Path) race 13 (Warrior group)
Cambridgeshire	16/199	2016	Red race 5 (Warrior group)
Cambridgeshire	16/204	2016	Red race 11 (Warrior group)
Cambridgeshire	16/205	2016	Red race 5 (Warrior group)
Cambridgeshire	16/208	2016	Blue race 7 (Warrior group)
Lincolnshire	16/131	2016	Red race 24 (Warrior group)
Lincolnshire	16/286	2016	Red race 23 (Warrior group)
Lincolnshire	16/288	2016	Red (Path) race 5 (Warrior group)
Lincolnshire	16/289	2016	Red race mix (Warrior group)
Lincolnshire	16/290	2016	Red race 23 (Warrior group)
Lincolnshire	16/292	2016	Pink race 14 (Warrior group)
Osgodby, Lincolnshire	16/277	2016	Blue race 10 (Warrior group)

Supplementary Table 1. Summary of *Pst* pathotypes identified from samples collected and tested by the UK Pathogen Virulence survey from Cambridgeshire and Lincolnshire in 2016 (Hubbard et al. 2017).

See Excel file

Supplementary Table 2. Glume yellow rust resistance phenotypic data (Best Linear Unbiased Estimators, BLUEs) in the wheat 'NIAB Elite MAGIC' population from trials NIAB15 and OSG16.

Site	REML estimates						σ^2e	h^2
	Random			Fixed				
	Term	Est.	SE	Term	Wald	*Chi pr*		
NIAB16	column	0.00137	0.0013	G	4227.1	<0.001	0.0603	0.80
OSG16	rep.block	0.00009	0.00043	G	4773.1	<0.001	0.0568	0.82

Supplementary Table 3. Summary of Restricted Maximum Likelihood (REML) covariance estimates of the mixed linear model for glume yellow rust resistance in the MAGIC population at trial sites NIAB16 and OSG16. Est.: estimates; SE: standard error; G: genotype; h^2: broad sense heritability; σ^2e: residual error.

See Excel file

Supplementary Table 4. Results of genetic mapping of glume yellow rust resistance in the wheat 'NIAB Elite MAGIC' population. 2016 season trial sites: NIAB (NIAB16) and Osgodby (OSG16). Results of four genetic mapping approaches are presented: (1) single marker analysis (SMA), (2) identity by descent (IBD), (3) interval mapping (IM), and (4) composite interval mapping with 10 covariates (CIM). For SMA and IBD, both *p*- and *q*-values are shown. For IM and IBD, the results presented are prior to model fitting.